Magnetic field tunable dielectric dispersion in successive field-induced magnetic phases of the geometrically frustrated magnet $CuFeO_2$ up to 28 T

H. Tamatsukuri,* S. Mitsuda, K. Hiroura, T. Nakajima,† M. Fujihala, M. Yamano, Y. Toshioka, and C. Kaneko
Department of Physics, Faculty of Science, Tokyo University of Science, Tokyo 162-8601, Japan

K. Takehana and Y. Imanaka
National Institute for Materials Science, Nano Physics Group, 3-13 Sakura, Tsukuba, Ibaraki 305-0003, Japan

N. Terada and H. Kitazawa
National Institute for Materials Science, Neutron Scattering Group, 1-2-1 Sengen, Tsukuba, Ibaraki 305-0047, Japan

(Received 24 January 2018; revised manuscript received 2 May 2018; published 7 June 2018)

We find magnetic-field-dependent dielectric dispersions specific to successive field-induced magnetic phases of a geometrically frustrated magnet $CuFeO_2$ up to 28 T. The dielectric dispersions in the three field-induced collinear-commensurate magnetic phases are well described by the superposition of Debye-type relaxations, and the number of contributions to the Debye-type dispersions differs in these phases. In contrast, the dielectric dispersions in the noncollinear-incommensurate phase, known as a spin-driven ferroelectric phase, cannot be simply described by the Debye-type relaxations. In addition, we find that the temperature dependence of the Debye relaxation frequencies follows the Arrhenius law, and that the activation energies derived from the Arrhenius equation also depend on the magnetic field. Considering the magnetostriction effect in combination with elongation/contraction of spins resulting from the application of a magnetic field, we show that the number of Debye relaxation components is equivalent to the number of states of local Fe_3O clusters determined by oxygen displacement within a triangular Fe lattice. Based on this correspondence, we propose a possible explanation that excess charges resulting from a lack of stoichiometry hop over the double-well potentials within each local Fe_3O cluster, like small polarons.

DOI: 10.1103/PhysRevB.97.214407

I. INTRODUCTION

The first discovery of so-called type-II multiferroics, in which magnetic ordering breaks the inversion symmetry of the system and generates ferroelectric polarization, resulted in a number of attempts to develop multifunctional electronic devices and to understand the underlying novel physical concepts [1–3]. Recently, there has been increasing interest in the dynamical aspects of the interplay between the magnetic and dielectric properties of solids. Dynamical coupling between magnetism and dielectricity not only has the potential to produce switching devices based on rapid manipulation of multiferroic states, but could also result in novel phenomena such as electromagnon excitation [3] and x-ray-induced phase transitions [4].

In this paper, we report a unique dynamical magnetocapacitance effect, in which an external magnetic field changes the complex permittivity (that is, the ac dielectric constant) of the geometrically frustrated magnetic delafossite $CuFeO_2$ (CFO), a known type-II multiferroic. Remarkably, the dielectric dispersions in CFO are modified in successive field-induced magnetic phases up to 28 T, indicating that the magnetic structure of CFO has a definite relationship with the dispersions.

The magnetic Fe^{3+} ions ($S = 5/2$) in CFO with antiferromagnetic interactions form triangular lattice layers stacked along the c axis, and this compound has been intensively investigated as a model material of geometrically frustrated magnets. As shown in Fig. 1, various studies have determined a highly rich temperature, T, vs. magnetic field, $\mu_0 H$, magnetic phase diagram for CFO [5–9]. Each of the magnetic orderings in Fig. 1 has a magnetic modulation wave vector (q,q,3/2). Note that hexagonal notation is used throughout this paper for convenience, although the magnetic phase transitions in CFO are accompanied by small spontaneous monoclinic lattice distortions [10–12]. In zero H and with decreasing T from a paramagnetic (PM) phase, the system enters a partially disordered (PD) phase at $T_{N1} = 14$ K and then a collinear 4-sublattice (4SL) phase at $T_{N2} = 11$ K. In the PD phase, the amplitude of spins along the c axis is sinusoidally modulated while, in the 4SL phase, the magnetic moments are oriented along the c axis in a two-up, two-down sequence [13,14]. When H is applied along the c axis below T_{N2}, CFO exhibits successive magnetic phase transitions: a ferroelectric-incommensurate magnetic (FE-ICM) phase (7 T $\lesssim \mu_0 H \lesssim$ 12 T) and a collinear 5-sublattice (5SL) phase with magnetic

*Present address: Institute of Materials Structure Science, High Energy Accelerator Research Organization (KEK), Tsukuba, Ibaraki 305-0801, Japan; hiromu.tamatsukuri@kek.jp
†Present address: RIKEN Center for Emergent Matter Science (CEMS), Saitama 351-0198, Japan.

 ©2018 American Physical Society

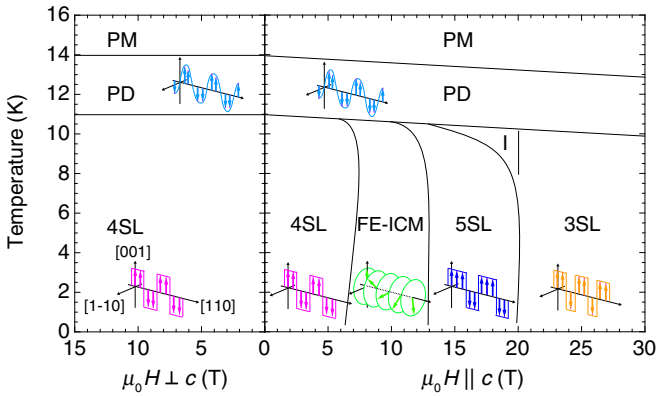

FIG. 1. Schematic H-T magnetic phase diagram for $CuFeO_2$, with H parallel or perpendicular to c axis. Although region I has been studied based on magnetization measurements, little is known about this phase (see Ref. [9]).

moments along the c axis in a three-up, two-down sequence ($12\ \mathrm{T} \lesssim \mu_0 H \lesssim 20\ \mathrm{T}$)[6]. In the FE-ICM phase, a screw helical magnetic structure, in which the screw axis is parallel to the [110] direction, is realized [15]. Because this helical magnetic structure breaks the spatial inversion symmetry of the system and generates ferroelectric polarization along the [110] direction through d-p hybridization [16,17], CFO is also known as the type-II multiferroics. Above $\mu_0 H \simeq 20$ T, a 1/3 plateau of the saturation magnetization phase appears [9]. Although the magnetic structure in this phase has not yet been directly determined, magnetization measurements strongly suggest that it has collinear 3-sublattice ordering in a two-up, one-down sequence [9]. Therefore, we refer to the 1/3 plateau phase as the 3SL phase. In contrast, when H is applied perpendicular to the c axis below T_{N2}, the 4SL phase persists up to 25 T [9].

A previous study observed magnetically tunable dielectric dispersions in the 4SL phase [18], and demonstrated that the relaxation frequency of these dielectric dispersions show anisotropic magnetic field dependence. It has been proposed that this phenomenon can be attributed to magnetic domain wall motion specific to the 4SL state and the corresponding displacement of oxygen ions near these walls. However, our own research has found that dielectric dispersions are also present in the other magnetic phases described above. Because the proposed magnetic domain wall motion is specific to the 4SL magnetic ordering, this model does not suitably account for dispersions in the other phases. In this study, instead of the magnetic domain wall motion model, we shed light on the origin of the magnetic-field-tunable dielectric dispersions in terms of the magnetostriction effect. Our proposal scenario can explain all of the field-dependent dielectric dispersions in successive field-induced magnetic phases of CFO.

II. EXPERIMENTS AND ANALYSES

Single crystals of CFO prepared by the floating zone method [19] were cut into thin disks (typically 20 $\mathrm{mm}^2 \times$ 0.3 mm), with the widest surfaces perpendicular to the c direction or the [110] direction. The electrodes consisted of silver paste painted onto these surfaces. Complex permittivity $\epsilon^*(\omega) \equiv \epsilon'(\omega) - i\epsilon''(\omega)$ was measured using a precision impedance analyzer (Agilent 4294A) or an LCR meter (Agilent E4980A). $H \parallel c$ was applied using a 15 T superconducting magnet or a hybrid magnet installed at the Tsukuba Magnet Laboratory in the National Institute for Materials Science. $H \perp c$ (along the [110] direction) was applied using the same 15 T superconducting magnet.

As described below, dielectric dispersions in the 4SL, 5SL, and 3SL phases are well fitted by a superposition of broadened Debye-type relaxations described by

$$\epsilon^*(\omega) = \epsilon'_\infty + \sum_n \frac{\Delta_n}{1 + (i\omega\tau_n)^{1-\alpha_n}}, \tag{1}$$

where ω, τ, and α are the angular frequency, the relaxation time and an empirical constant accounting for a distribution of relaxation times ($\alpha = 0$ corresponds to the Debye model), respectively, and n represents the number of contributions to the superposition, which differs in each of the phases. For simplicity, we introduce $\Delta_n \equiv \epsilon'_{0n} - \epsilon'_\infty$, where ϵ'_{0n} and ϵ'_∞ are the static- and high-frequency limiting values of the dielectric constant, respectively. Note that Eq. (1) produces a semicircular arc in the ϵ'-ϵ'' plane, which is known as a Cole-Cole plot [20].

We analyze the temperature dependence of τ according to the Arrhenius law:

$$\tau = \tau_0 \exp(E_a / k_B T), \tag{2}$$

where τ_0, k_B, and E_a are a coefficient, the Boltzmann constant and the activation energy. The latter equals the height of the double-well potential barrier separating two local minima.

III. RESULTS

A. The 4SL phase

Figures 2(a) to 2(f) show the typical dielectric dispersions in the 4SL phase at selected temperatures. At zero H, the dispersion is well described by only one component of the Debye-type dispersion. When $\mu_0 H \parallel c \geqq 4$ T is applied, the dispersion spectra drastically change [Figs. 2(c) and 2(d)]. The Cole-Cole plot for $\mu_0 H \parallel c = 5$ T shown in Fig. 2(g) clearly indicates that the dispersions in $H \parallel c$ can be characterized as the superposition of two kinds of Debye-type contributions. In fact, as shown in Figs. 3(a) and 3(b), the dispersions under $H \parallel c \geqq 4$ T are well fitted by the two component Debye-type relaxations. In contrast, in the case of $H \perp c$ up to 15 T, no splitting of ϵ'' was observed [Figs. 2(e) and 2(f)]. These results demonstrate that the dielectric dispersions in the CFO exhibit significant anisotropy with respect to the external magnetic field. These features are consistent with previously reported results [18].

Moreover, we find that the T dependence of the peak positions, τ_n, follows the Arrhenius law, as shown in Figs. 3(c) and 3(d). This result allows us to introduce an activation energy, E_a, for each dispersion. It was determined that the E_a value derived from τ_1 increases with increasing H, while the E_a derived from τ_2 is almost independent of H. In the case of $H \perp c$, E_a moderately increases with increasing H.

It should be noted that the difference in $\epsilon'(\omega \to 0)$ between $\mu_0 H = 0$ T and $\mu_0 H \parallel c = 5$ T is not attributed to the

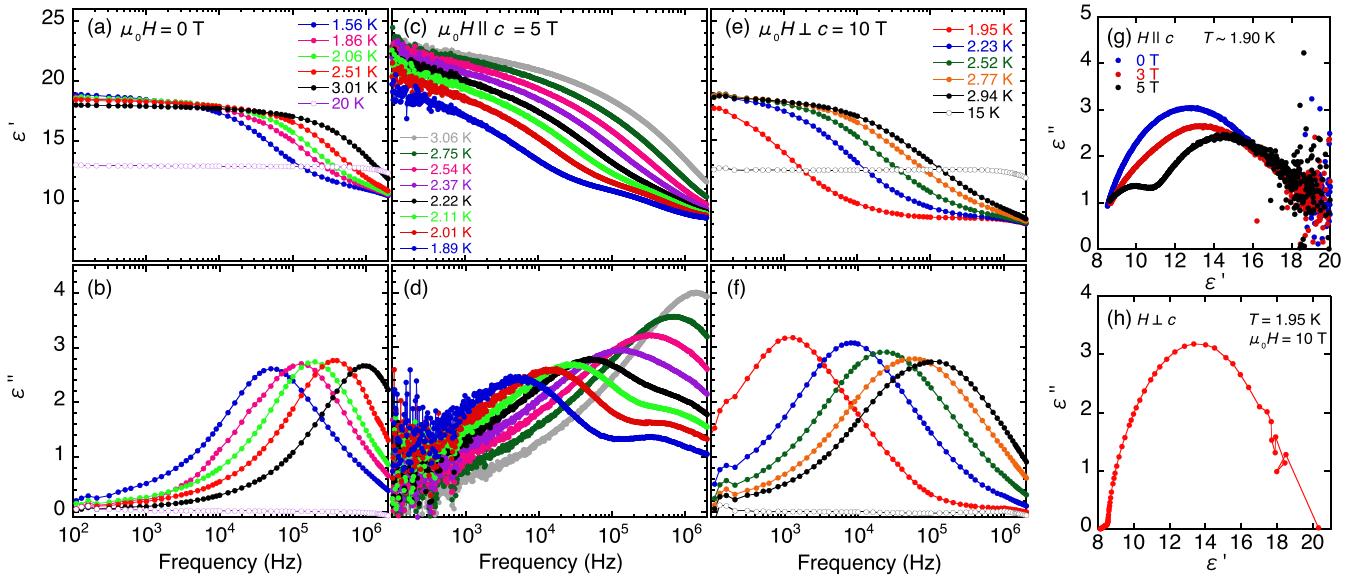

FIG. 2. Typical dielectric dispersions in the 4SL phase at selected temperatures for (a–b) zero H, (c–d) $\mu_0 H \parallel c = 5$ T, and (e–f) $\mu_0 H \perp c = 10$ T. Cole-Cole plots at the lowest temperatures for (g) $H \parallel c$ and (h) $H \perp c$.

application of H but rather to variations in the experimental conditions, such as the electrodes employed, or possibly differences in the samples. Conversely, τ_n is independent of the experimental conditions and essentially constant between samples. In the following sections, therefore, we primarily focus on T dependence of τ and H dependence of E_a. The values of Δ_n, ϵ'_∞ obtained by the fitting are summarized in Sec. A.

B. The 5SL phase

Figures 4(a) and 4(b) demonstrate the typical temperature dependence of the dielectric dispersions in the 5SL phase. These dispersions are characterized by a superposition of three Debye-type contributions, as evidenced by the fitting results [Figs. 4(a) and 4(b)] and the Cole-Cole plot [Fig. 4(c)]. The Cole-Cole plot for the results in the 5SL phase does not exhibit a series of clear semicircles, in contrast to the results obtained for the 4SL phase. This is attributed to the overlap of spectra and we were able to obtain reasonable values by fitting using Eq. (1) ($n = 3$) (see Sec. A). As in the 4SL phase, all three τ obtained by the fitting conform to the Arrhenius relationship, as shown in Fig. 4(d).

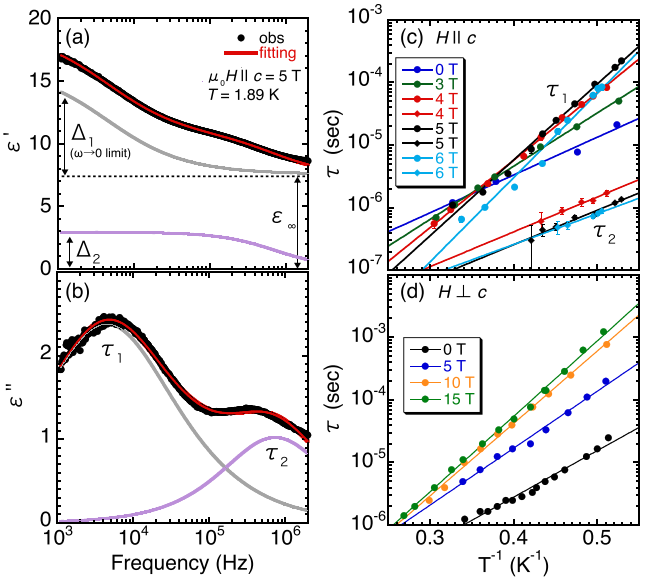

FIG. 3. (a–b) Typical results of fitting to Eq. (1) ($n = 2$, $T = 1.89$ K, $\mu_0 H \parallel c = 5$ T). Arrhenius plots for (c) $H \parallel c$ and (d) $H \perp c$.

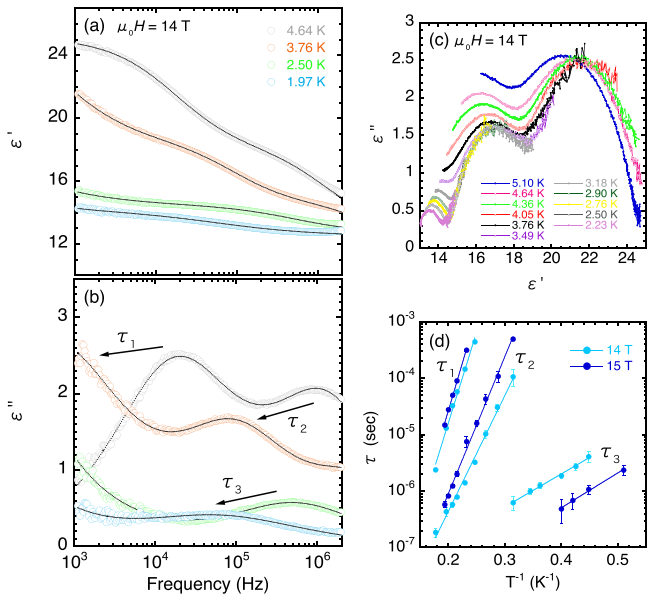

FIG. 4. (a–b) Typical dielectric dispersions in the 5SL phase at selected temperatures under $\mu_0 H \parallel c = 14$ T. The solid black curves are fitting results ($n = 3$). (c) Cole-Cole plots at selected temperatures for $\mu_0 H \parallel c = 14$ T. (d) Arrhenius plot for $\mu_0 H \parallel c = 14$ and 15 T.

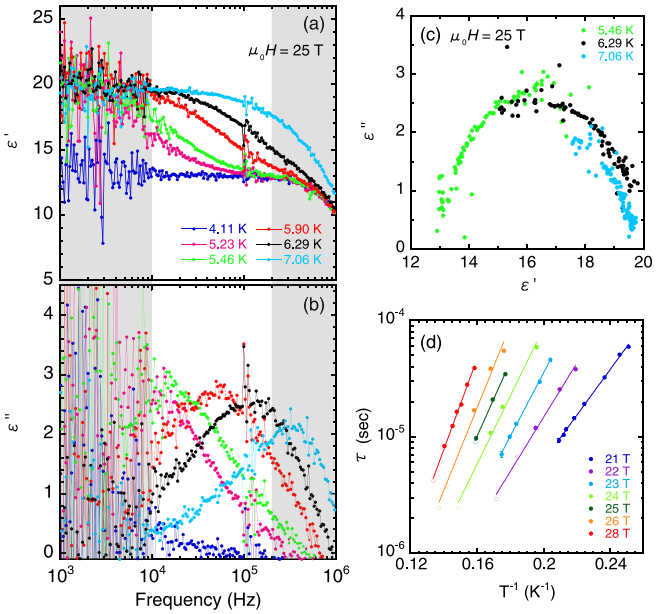

FIG. 5. (a–b) Typical dielectric dispersions in the 3SL phase at selected temperatures under $\mu_0 H \parallel c = 25$ T. The areas shaded gray indicate frequency ranges disturbed by noise from the hybrid magnet (primarily the low-frequency region) and the long coaxial cable (primarily the high frequency region). (c) Cole-Cole plots at selected temperatures for $\mu_0 H \parallel c = 25$ T. (d) The Arrhenius plots for data in the 3SL phase. The values indicated by open symbols were obtained by fitting with certain fixed parameters (see Sec. A).

C. The 3SL phase

In Figs. 5(a) and 5(b), we show the typical temperature dependence of dielectric dispersions in the 3SL phase. To access the 3SL phase ($H \geqslant 20$ T), we employ the hybrid magnet and a long coaxial cable ($\sim$10 m). Because the complex permittivity measurements were extremely sensitive to noise from these devices, the usable frequency region was quite limited compared to the data range for the 4SL and 5SL phases. However, despite this limited range, we were able to characterize the dispersions in the 3SL phase as Debye-type with a single component, based on the symmetric spectra and the Cole-Cole plot [Fig. 5(c)]. Model fitting could also be performed [Sec. A]. As shown in Fig. 5(d), τ in the 3SL phase obeys the Arrhenius law, similar to the case for the 4SL and 5SL phases.

D. The FE-ICM phase

Figures 6(a) and 6(b) demonstrate the typical frequency dependence of the complex permittivity in the FE-ICM phase. We observed rather broad dispersions that are dependent on T and H, as is also the case for the other collinear phases. In contrast to the collinear phases, however, the dispersions in the FE-ICM phase cannot be simply described by the Debye-type relaxations. In fact, the Cole-Cole plots for the results in the FE-ICM phase do not show a semicircular arc [see Fig. 6(c)]. These results suggest that collinear magnetic structures are an essential prerequisite for Debye-type dispersions in CFO. Although the dispersions in the FE-ICM phase can not be fitted by Eq. (1) with two or more components, we find that

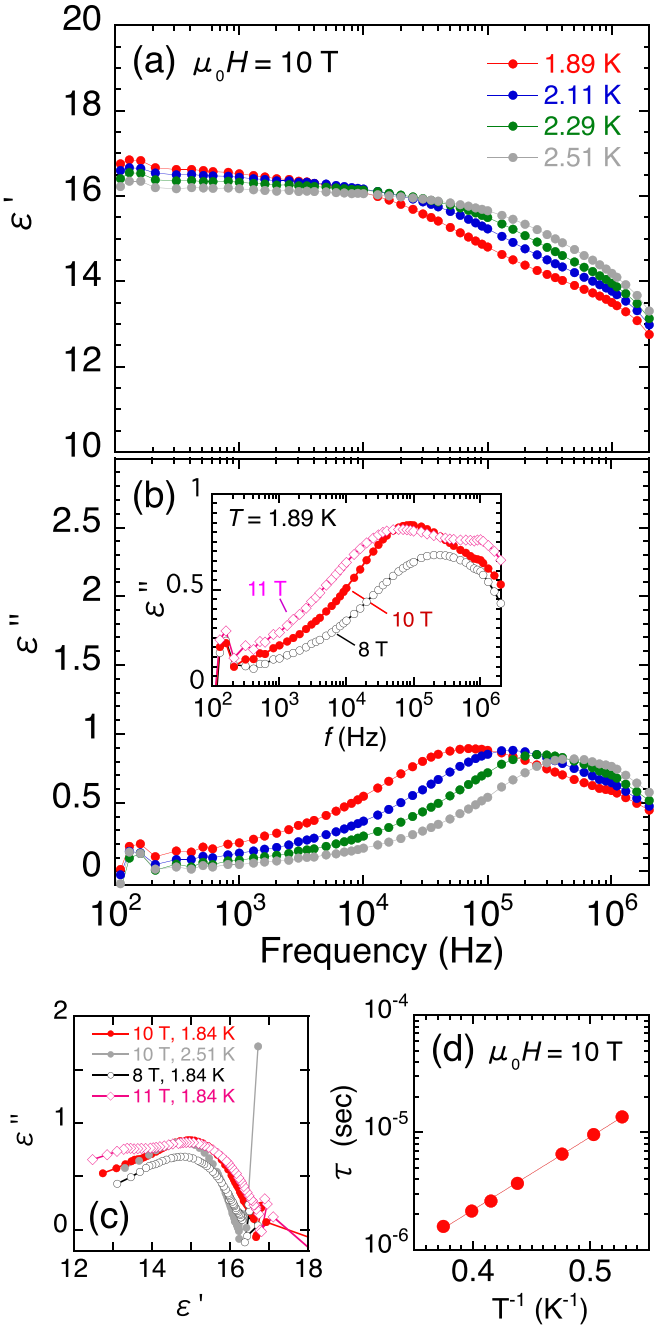

FIG. 6. Frequency dependence of (a) real and (b) imaginary parts of ϵ^* in the FE-ICM phase at selected temperatures under $\mu_0 H \parallel c = 10$ T. The insets to (a) and (b) show Cole-Cole plots at several T and H for the FE-ICM phase and the frequency dependence of the imaginary part at several H and the lowest temperature, respectively.

the temperature dependence of frequencies where ϵ'' shows a maximum follows the Arrhenius law.

We also note that no dielectric dispersions were observed in the PD phase for any value of H (not shown).

IV. DISCUSSION

Let us discuss the origin of the field-dependent dielectric dispersions. In a previous study [18], as mentioned in Sec. I,

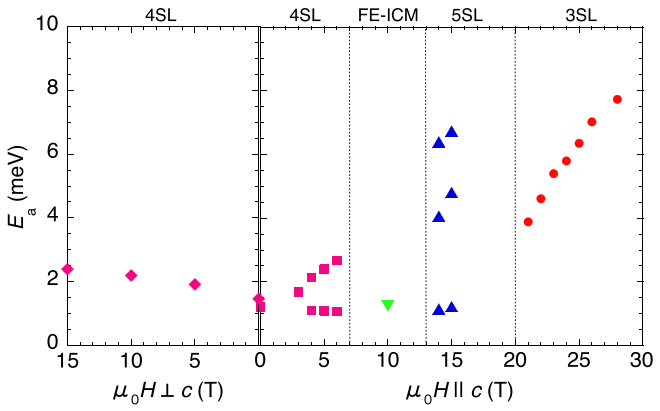

FIG. 7. Magnetic field dependence of activation energy values obtained using Arrhenius law. Note that, although the 5SL phase beyond 15 T could be accessed using the hybrid magnet, it was extremely difficult to perform the Debye model fitting with three components due to the limited frequency range.

the authors proposed a naive scenario for the appearance of magnetically tunable dielectric dispersions in the 4SL phase. In this mechanism, the magnetostriction effect [21] causes an oxygen ion at the center of the triangular lattice to move so as to gain superexchange energy, resulting in an "antiferroelectric" three-dimensional alignment of dipole moments. The induced electric dipole moments near sequence domain walls, at which the 4SL magnetic ordering sequence is broken and another sequence starts, can oscillate in space under an applied ac-electric field and generate the dielectric dispersions if accompanied by a back-and-forth movement of the walls.

To consider the back-and-forth movement of the domain walls in terms of an activation energy, we show the magnetic field dependence of E_a values obtained using the Arrhenius law in Fig. 7. These values range from 1 $\sim$ 10 meV. Since $E_a = 1.5$ meV at $H = 0$ T, for example, corresponds to $\sim$17 K, at which CFO exhibits no magnetic ordering, we can consider that the back-and-forth movement of the domain walls should not occur down to 2 K. These results strongly suggest that the dielectric dispersions in CFO does not originate from the domain wall motion. Moreover, the original naive scenario does not explain the anisotropic H dependence of the relaxation frequencies in the 4SL phase.

Here, we propose an alternative explanation for the appearance of field-dependent dielectric dispersions. Taking into account the elongation/contraction of spins upon the application of H, we develop the above idea that the oxygen ion moves from the original center position due to the magnetostriction effect, although we do not associate this oxygen ion displacement with the domain wall motion. As shown in Fig. 8(a), at zero H, there are two kinds of spin arrangement on the triangular lattice in the 4SL $\uparrow\uparrow\downarrow\downarrow$ ordering. Since the oxygen moves from the parallel-spin side toward the antiparallel-spin corner according to the magnetostriction effect [21], the oxygen ion displacement within the triangular lattice is equivalent in both types of Fe_3O clusters. Taking into account that there are suppression of the magnetic moments by the geometrical frustration even in the 4SL ground state [22], the application of $H \parallel c$ would cause the suppressed moments parallel (antiparallel) to the H

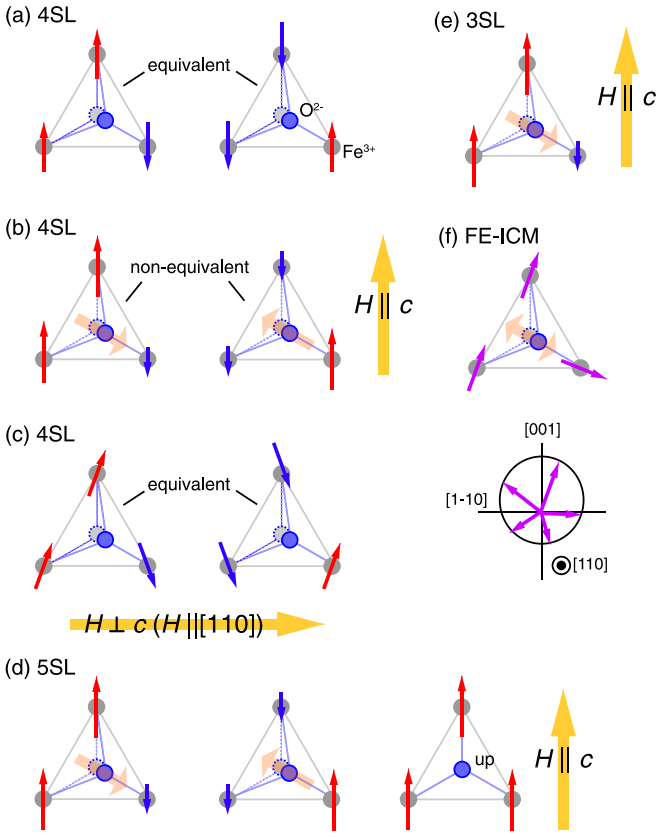

FIG. 8. (a) Two different Fe_3O clusters with spin arrangements on the triangular lattice in the 4SL phase. Due to the magnetostriction effect [21], the oxygen ion moves from the parallel-spin side toward the antiparallel-spin corner. States of the Fe_3O clusters in the 4SL phase under (b) $H \parallel c$ and (c) $H \perp c$. The solid orange arrows in (b) indicate the expected direction of oxygen displacement in response to $H \parallel c$. Fe_3O clusters in the (d) 5SL, (e) 3SL, and (f) FE-ICM phases. The bottom panel of (f) shows a [001]-[1$\bar{1}$0]-plane-projection of the magnetic moments with a helical arrangement in the FE-ICM phase.

direction to elongate (contract). This elongation/contraction of the moments leads to further movement of the oxygen ions [Fig. 8(b)]. As a result, the displacements of the oxygen ions within the triangular lattice become nonequivalent. Note that, for the sake of simplicity, we assume that only the oxygen ions are displaced [23]. In contrast, in response to the application of $H \perp c$, the magnetic moments incline toward the direction of H because magnetization linearly increases with increasing $H \perp c$ [9,12]. This indicates that the state of the two Fe_3O clusters remain equivalent in energy, although the oxygen ions are further moved [Fig. 8(c)]. In the case of the 5SL and 3SL phases, three and one states appear for the Fe_3O clusters under $H \parallel c$, respectively [Figs. 8(d) and 8(e)]. Therefore, the number of Debye relaxation components (or E_a) in each collinear phase directly corresponds to the number of local Fe_3O cluster classes. On the basis of this correspondence, we speculate that each local Fe_3O cluster generates double-well potentials within itself, and some excess charges resulting from nonstoichiometry, such as oxygen vacancies, hop over the double-well potentials owing to the applied ac-electric field. That is, these magnetic orderings provide the local environment

that determines the response to an applied ac-electric field, while the respondents are common to these magnetic phases.

This classification of the state of the Fe_3O clusters under $H \parallel c$ is also applicable to the FE-ICM phase. Because two of the three spins are parallel within the Fe_3O clusters, the direction of oxygen ion displacement in the FE-ICM phase is the same as that in the 4SL phase [Fig. 8(f)] [21]. However, as shown in Fig. 8(f) lower panel, the elongation/contraction of spins upon the application of H in the FE-ICM phase varies with the spin orientation relative to H. Therefore, in contrast to the 4SL phase, the state of the Fe_3O clusters in the FE-ICM phase cannot be divided into two classes, meaning that the Fe_3O clusters may exist in many states. This results in the nonsimple Debye-type dispersions in the FE-ICM phase which, nevertheless, may be regarded as continuously distributed Debye-type broad dispersions. This would also be consistent with the facts that the temperature dependence of the peak top frequencies in ϵ'' obeys the Arrhenius law even in the FE-ICM phase, and that the E_a value in the FE-ICM phase is comparable to those in the other phases. Moreover, the above scenario is consistent with our experimental observation that no dielectric dispersion was observed in the PD phase because uniform oxygen displacement has not been reported in this phase [21].

There are several compounds that exhibit H-dependent Debye-type dielectric dispersions [24–27]. The dielectric dispersions in $DyMnO_3$, whose magnitude can be controlled by varying H, show the greatest strength in a spin flop transition magnetic field. These can be well explained by the local motion of the multiferroic domain walls between bc-plane spin cycloid ($\boldsymbol{P} \parallel c$) and ab-plane spin cycloid ($\boldsymbol{P} \perp c$) domains (where $\boldsymbol{P}$ is the ferroelectric polarization) [24,25]. $Y_3Fe_5O_{12}$ (yttrium iron garnet, YIG) exhibits dielectric relaxation due to quantum paraelectricity, and the magnitude of this relaxation can be enhanced by the application of H [26,27]. Although E_a in $DyMnO_3$ and YIG is not explicitly described in the literature, we can estimate values from the Arrhenius plots that have been reported. The resulting values are $\sim$0.75 meV for $DyMnO_3$ [24] and $\sim$0 eV for YIG, because the relaxation frequencies in YIG are almost independent of T ($\sim$100 Hz) [26]. As shown in Fig. 7, the E_a values for CFO are much higher than those for $DyMnO_3$ and YIG. Therefore, the dielectric dispersions in CFO are much more thermally active than those in $DyMnO_3$ and YIG. This result would corroborate our proposed mechanism in which dielectric dispersions in CFO originate from the hopping of excess charges like small polarons, and not from local domain wall motions as in $DyMnO_3$ nor quantum tunneling as in YIG. To further confirm our scenario, complex permittivity measurements using precisely carrier-controlled samples would be helpful.

Our proposed scenario has the advantage of reasonably explaining the anisotropic H dependence of the relaxation frequencies in the 4SL phase, and is also applicable to the nonsimple-Debye-type dispersions in the FE-ICM phase. However, there are several fundamental questions in this phenomenon and in our scenario. In our analyses of the relaxation processes, instead of looking at the H variation of τ_n values itself at fixed temperatures, these are characterized by the the H variation of E_a and τ_0 through the Arrhenius law. Even though we obtained the systematic H dependence of E_as using the Arrhenius law, it is also difficult to discuss why E_{a1} and E_{a2} in the 5SL phase increase with increasing H, whereas E_{a3} is almost independent of H (see Fig. 7), and to discuss the H variation of τ_0. Similar features are also seen in the 4SL and 3SL phases [Figs. 3(c), 3(d), 5(d), and 7). In addition, our proposed scenario leads us to ask which E_a branches correspond to modes of the double-well potentials generated in each local Fe_3O cluster. Moreover, as noted above, the frequency range of the measurements was limited, especially in the case of the 3SL phase. To completely understand this phenomenon, further investigations including theoretical calculations should be performed.

V. SUMMARY

We investigate dielectric dispersions in successive field-induced magnetic phases of the geometrically frustrated magnet $CuFeO_2$, up to 28 T. The dielectric dispersions in the 4SL, 5SL, and 3SL (collinear-commensurate) phases under applied $H \parallel c$ are well characterized by Debye-type relaxations with two, three, and one components, respectively. In contrast, the dielectric dispersions in the 4SL phase under applied $H \perp c$ are described by a single Debye-type relaxation. The dielectric dispersions in the FE-ICM (noncollinear-incommensurate) phase cannot be simply described by the Debye-type relaxations. These results indicate that collinear-commensurate magnetic structures are essential for the dielectric dispersions in CFO to exhibit Debye-type relaxation. We also find that the temperature dependence of the Debye relaxation frequencies follows the Arrhenius law, and that the activation energies E_a, derived from the Arrhenius relationship depend on the magnetic field.

Considering the magnetostriction effect, in combination with the elongation/contraction of spins in response to an applied H, the number of Debye relaxation components (or E_a) completely corresponds to the number of states of local Fe_3O clusters. We suggest that some excess charges that appear due to nonstoichiometric conditions hop over the double-well potentials within each local Fe_3O cluster, like a small polarons hopping. Although this scenario provides a reasonable explanation of the anisotropic H dependence of the relaxation frequencies in the 4SL phase, and is also applicable to the non-Debye-type dispersions in the FE-ICM phase, the relationship between E_a and the double-well potentials generated in each local Fe_3O cluster should be clarified. The unique dynamical magnetocapacitance effect in CFO evidently provides an opportunity to investigate coupling between magnetic ordering and electric dipole fluctuations without spin-driven ferroelectricity.

ACKNOWLEDGMENTS

This work was supported by the NIMS Joint Research Hub Program and by Grants-in-Aid for Scientific Research (C) (No. 23540424 and No. 26400369) from the Japan Society for the Promotion of Science.

APPENDIX A: FITTING RESULTS

The typical values obtained from the fitting procedure are summarized in Figs. 9(a) to 9(f). In the case of the 4SL and

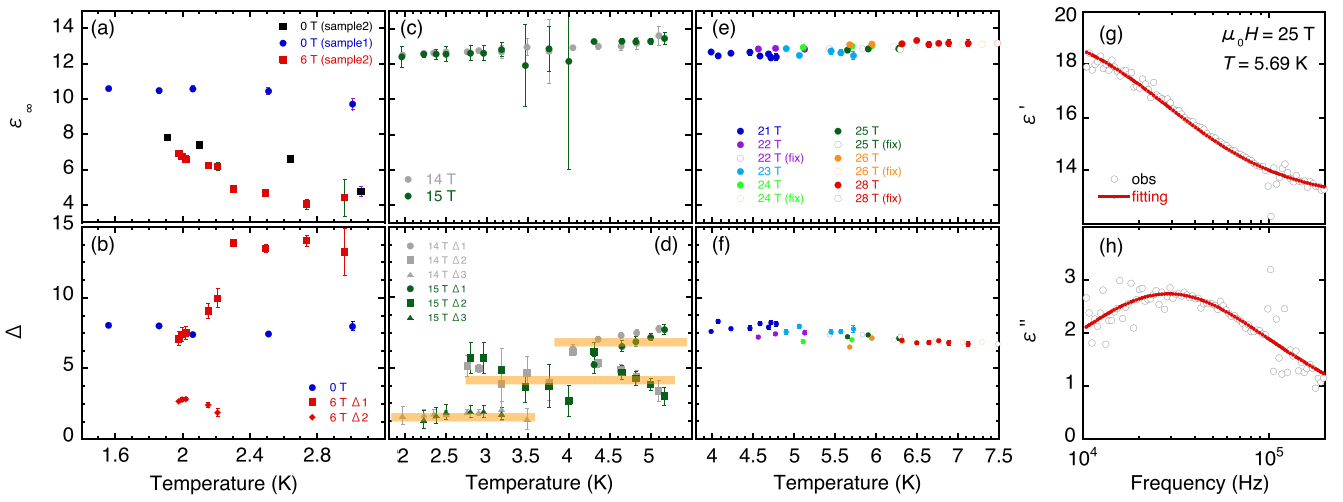

FIG. 9. Typical values of ϵ_∞ and Δ obtained by a fitting procedure for the (a–b) 4SL, (c–d) 5SL, and (e–f) 3SL phases. Solid lines in (d) are visual guides and open symbols indicate fixed values used in fitting. (g–h) Typical fitting results for the 3SL phase ($n = 1$, $T = 5.69$ K, $\mu_0 H \parallel c = 25$ T).

5SL phases, we did not restrict the parameters used in fitting. Although the temperature dependence of Δ_n exhibits some scatter due to the correlation between Δ_ns and ϵ'_∞, we can say that Δ_n is almost independent of T [Figs. 9(b) and 9(d)]. For the 3SL phase data, we partly use fixed values, which are estimated based on values obtained by fitting with all the free parameters because of the limited frequency range noted in the main text. Typical fitting results for the data in the 3SL phase are shown in Figs. 9(g) and 9(h). Here, α ranges from 0.2 to 0.5, from 0.15 to 0.4, and from 0.15 to 0.3, in the 4SL, 5SL, and 3SL phases, respectively.

At this point, we wish to suggest an appropriate interpretation of ϵ'_∞ and Δ_n. As shown in Figs. 9(a), 9(c), and 9(e), the $\epsilon'_\infty \simeq 11$ of sample 1 in the 4SL phase is comparable to those in the 5SL and 3SL phases. Because ϵ'_∞ should reflect only the lattice dynamics of this compound [with no contribution due to the response of (induced) dipole moments or excess charges], we consider that $\epsilon'_\infty \simeq 12$ is essentially independent of T and H. However, ϵ'_∞ and Δ_n appears to vary from sample to sample in the 4SL phase [Figs. 9(a) and 9(b)]. We believe that this discrepancy originates from the condition of the silver paste electrodes. Moreover, there is the possibility that Δ_n satisfies the sum rule in each phase, and the summation value, ~8, is preserved across the successive field-induced magnetic phases since Δ should depend on the density of the (induced) dipole moments. The summation value of Δ_n in the 5SL phase may be larger than those in the other phases because of the condition

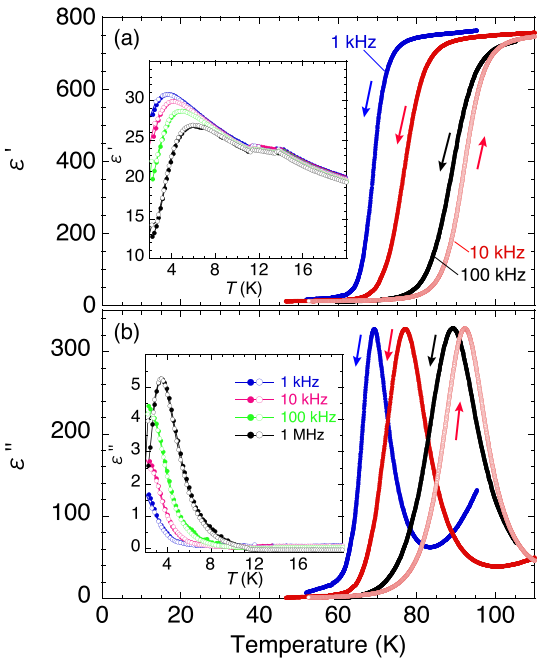

FIG. 10. Temperature dependence of (a) ϵ' and (b) ϵ''. Insets show magnifications of these data in the low-temperature region.

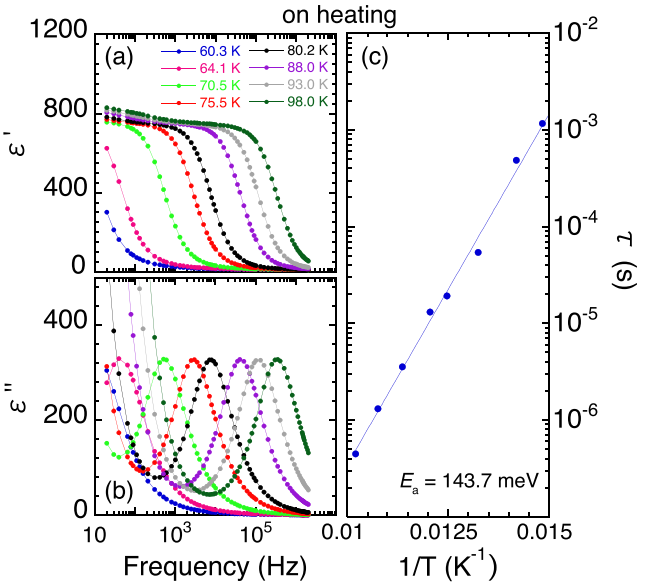

FIG. 11. Frequency dependence of (a) ϵ' and (b) ϵ'' determined by heating trials in high-temperature region. (c) Arrhenius plots for Debye-like dispersions in the high temperature.

of the electrodes. Although the above interpretation of ϵ'_∞ and Δ_n agrees with our proposed mechanism, these points should be confirmed using a more precise technique for fabricating the electrodes.

APPENDIX B: TEMPERATURE DEPENDENCE OF ϵ^* AND DIELECTRIC DISPERSIONS IN A HIGH-TEMPERATURE REGION

The temperature dependence of ϵ^* at selected frequencies in the high-temperature region is summarized in Figs. 10(a) and 10(b). We find that ϵ' exhibits large, steep step-like variations in conjunction with a high degree of hysteresis over ~20 K, and the characteristic temperature shifts to higher temperatures with increasing frequency. ϵ'' also shows a peak at the characteristic temperature.

Figures 11(a) and 11(b) show the frequency dependence of ϵ' and ϵ'' in the high-temperature region. Both exhibit Debye-like behavior, except for the $1/\omega$ contribution to ϵ'', which originates from conductivity (since CFO is an intrinsic semiconductor). We attempt to analyze the frequency dependence of the Debye-like dispersions using Eq. (2), and obtained an activation energy of 143.7 meV. Also, we confirm that the dielectric dispersions in the high-temperature region are independent of H (data not shown).

The characteristic temperature and the activation energy varied in each experiment. These results suggest that the Maxwell-Wagner effect is the origin of the temperature/frequency dependence of ϵ^* in the high-temperature region [28,29]. The Maxwell-Wagner effect originates from grain boundaries and/or the interface between a sample and an electrode, and results in Debye-like dispersions. Therefore, the dielectric dispersions in the high-temperature region may not be intrinsic to CFO. Conversely, the temperature dependence of ϵ^* in the low-temperature region is almost sample-independent [see the insets to Figs. 10(a) and 10(b)]; therefore, the dielectric dispersions in this study are undoubtedly intrinsic to CFO.

[1] T. Kimura, T. Goto, H. Shintani, K. Ishizaka, T. Arima, and Y. Tokura, Nature (London) **426**, 55 (2003).

[2] M. Fiebig, J. Phys. D: Appl. Phys. **38**, R123 (2005).

[3] Y. Tokura, S. Seki, and N. Nagaosa, Rep. Prog. Phys. **77**, 076501 (2014).

[4] Y. Yamasaki, H. Nakao, Y. Murakami, T. Nakajima, A. L. Sampietro, H. Ohsumi, M. Takata, T. Arima, and Y. Tokura, Phys. Rev. B **91**, 100403 (2015).

[5] S. Mitsuda, M. Mase, T. Uno, H. Kitazawa, and H. A. Katori, J. Phys. Soc. Jpn. **69**, 33 (2000).

[6] S. Mitsuda, M. Mase, K. Prokes, H. Kitazawa, and H. A. Katori, J. Phys. Soc. Jpn. **69**, 3513 (2000).

[7] O. A. Petrenko, M. R. Lees, G. Balakrishnan, S. de Brion, and G. Chouteau, J. Phys. Condens. Matter **17**, 2741 (2005).

[8] G. Quirion, M. L. Plumer, O. A. Petrenko, G. Balakrishnan, and C. Proust, Phys. Rev. B **80**, 064420 (2009).

[9] T. T. A. Lummen, C. Strohm, H. Rakoto, and P. H. M. van Loosdrecht, Phys. Rev. B **81**, 224420 (2010).

[10] F. Ye, Y. Ren, Q. Huang, J. A. Fernandez-Baca, P. Dai, J. W. Lynn, and T. Kimura, Phys. Rev. B **73**, 220404(R) (2006).

[11] N. Terada, S. Mitsuda, H. Ohsumi, and K. Tajima, J. Phys. Soc. Jpn. **75**, 023602 (2006).

[12] N. Terada, Y. Narumi, Y. Sawai, K. Katsumata, U. Staub, Y. Tanaka, A. Kikkawa, T. Fukui, K. Kindo, T. Yamamoto, R. Kanmuri, M. Hagiwara, H. Toyokawa, T. Ishikawa, and H. Kitamura, Phys. Rev. B **75**, 224411 (2007).

[13] M. Mekata, N. Yaguchi, T. Takagi, T. Sugino, S. Mitsuda, H. Yoshizawa, N. Hosoito, and T. Shinjo, J. Phys. Soc. Jpn. **62**, 4474 (1993).

[14] S. Mitsuda, N. Kasahara, T. Uno, and M. Mase, J. Phys. Soc. Jpn. **67**, 4026 (1998).

[15] T. Nakajima, S. Mitsuda, S. Kanetsuki, K. Prokes, A. Podlesnyak, H. Kimura, and Y. Noda, J. Phys. Soc. Jpn. **76**, 043709 (2007).

[16] T. Nakajima, S. Mitsuda, S. Kanetsuki, K. Tanaka, K. Fujii, N. Terada, M. Soda, M. Matsuura, and K. Hirota, Phys. Rev. B **77**, 052401 (2008).

[17] T. Arima, J. Phys. Soc. Jpn. **76**, 073702 (2007).

[18] S. Mitsuda, M. Yamano, K. Kuribara, T. Nakajima, K. Masuda, K. Yoshitomi, N. Terada, H. Kitazawa, K. Takehaka, and T. Takamasu, J. Phys. Conf. Ser. **200**, 012120 (2010).

[19] T. R. Zhao, M. Hasegawa, and H. Takei, J. Cryst. Growth **166**, 408 (1996).

[20] K. S. Cole and R. H. Cole, J. Chem. Phys. **9**, 341 (1941).

[21] N. Terada, S. Mitsuda, Y. Tanaka, Y. Tabata, K. Katsumata, and A. Kikkawa, J. Phys. Soc. Jpn. **77**, 054701 (2008).

[22] Neutron diffraction studies revealed that a magnetic moment at 4.2 K is ~4.2 μ_B (full moment is 5 μ_B for Fe^{3+} ($S = 5/2$)) even in the 4SL ground state [10,13], and magnetization in the 4SL phase slightly increases with increasing $H \parallel c$ [9,12].

[23] Note that the triangular lattice of Fe^{3+} ions is distorted in the 4SL phase, as briefly mentioned in Sec. I, and the application of H ($\parallel$ and $\perp$ c) restores the distorted triangular Fe lattice toward an equilateral one[12]. Besides the Fe triangular lattice distortion, a displacement of oxygen ions within the Fe triangular lattice can also be considered to occur, as evidenced by observation of the superlattice reflections[21]. We assume this phenomenon in our scenario.

[24] F. Kagawa, M. Mochizuki, Y. Onose, H. Murakawa, Y. Kaneko, N. Furukawa, and Y. Tokura, Phys. Rev. Lett. **102**, 057604 (2009).

[25] F. Kagawa, Y. Onose, Y. Kaneko, and Y. Tokura, Phys. Rev. B **83**, 054413 (2011).

[26] Y. Yamasaki, Y. Kohara, and Y. Tokura, Phys. Rev. B **80**, 140412 (2009).

[27] Y. Kohara, Y. Yamasaki, Y. Onose, and Y. Tokura, Phys. Rev. B **82**, 104419 (2010).

[28] P. Lunkenheimer, V. Bobnar, A. V. Pronin, A. I. Ritus, A. A. Volkov, and A. Loidl, Phys. Rev. B **66**, 052105 (2002).

[29] R. Schmidt, J. Ventura, E. Langenberg, N. M. Nemes, C. Munuera, M. Varela, M. Garcia-Hernandez, C. Leon, and J. Santamaria, Phys. Rev. B **86**, 035113 (2012).